Orbital
The electronic journal of chemistry

the electronic journal of chemistry

Full paper | http://dx.doi.org/10.17807/orbital.v17i1.20314

Structural Elucidation, DFT Calculations, Hirshfeld Surface Analysis, Molecular Dynamics Simulation, ADMET Profiles, and Molecular Docking of Two Benzazocine Derivatives NAOP-12 and NEMKH-12

Tanveer Hasan*[a], Raza Murad Ghalib [b], Sayed Hasan Mehdi [c], Tazeem [c], and Nazia Kazmi [d]

In this study two novel benzazocine derivatives containing potentially anticancer properties, (a) NAOP-12 ($C_{24}H_{16}N_4$) & (b) NEMKH-12 ($C_{25}H_{18}N_4$), were investigated utilizing quantum computational technique. The equilibrium geometries of the compounds have been obtained and analyzed using the DFT-B3LYP/6-311++G(d,p) method. FT-IR analysis was used to identify the various functional groups, and the results are compared to the simulated spectra. The oscillation modes were examined theoretically. The electronic properties such as HOMO and LUMO energies and associated frontier energy band gap were calculated. Molecular Electrostatic Potential predictions are done to analyze the electrophilic and nucleophilic centers. Electrical parameters like dipole moment, molecular polarizability and first static hyperpolarizability, have been utilized to predict the biological nature and non-linear optical (NLO) behavior of the molecules. Chemically active sites are described using Fukui functions, chemical softness, and other descriptors. The Hirshfeld surface analysis has been performed to investigate the weak interactions in the molecules. A 500 ns molecular dynamics simulation was conducted, evaluating models using RMSD, RMSF, Rg, SASA metrics and the gmxMMPBSA tool was utilized for free energy calculations. The molecular docking analysis has been performed with the fusion proteins 6J7A and 6J7I. The drug-likeness and ADMET parameters were computed to investigate their pharmaceutical behavior.

Graphical abstract

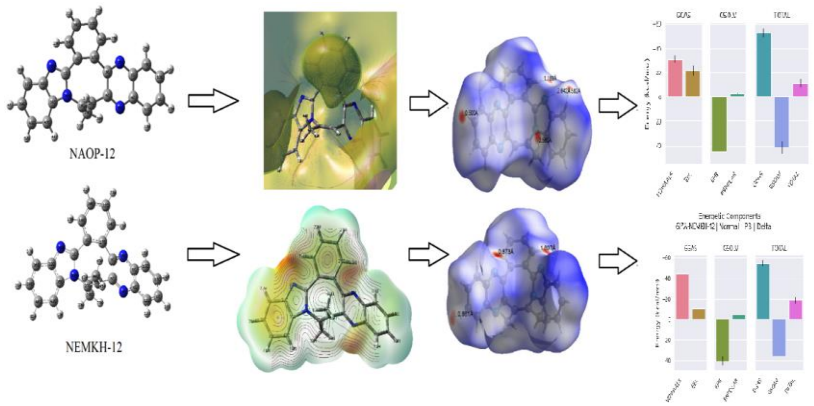

Keywords

Molecular Dynamics
Molecular Docking
ADMET
DFT
Fukui functions
Hirshfeld surface

Article history

Received 03 Mar 2024
Revised 28 Feb 2025
Accepted 14 Apr 2025
Available online 26 Apr 2025

Handling Editor: Arlan Gonçalves

[a] Deptt. of Physics, Shia P.G. College, Lucknow-226020, India. [b] Deptt. of Chemistry, Faculty of Sciences & Arts, Khulais, University of Jeddah, P.O. Box 355, Postal Code 21921 Jeddah, KSA. [c] Deptt. of Chemistry, Shia P. G. College, Lucknow-226020, India. [d] Deptt. of Zoology, Shia P.G. College, Lucknow-226020, India. *Corresponding author. Email: **tanveerhasan09@gmail.com**

1. Introduction

Cancer research is leading to a multitude of breakthroughs in its prognosis. The process of drug discovery is truly multidisciplinary in nature as it sets a platform to work together for experts from the diverse fields. Fusion proteins which are results of expression of genes from different chromosomes getting accidentally fused are a new focus of cancer therapeutics [1]. Breakage of chromosomes and their fusion to form oncoproteins is well documented in case of several cancers especially those occurring in childhood. Several fusion proteins of this kind have been shown to not only existing tumours but have been identified as the major trigger for uncontrolled cell division. Experts believe that fusion proteins can be decisive targets for novel drugs which can be exploited to prevent the progression of cancers by nipping them in the bud. This perspective has been applied successfully in treating chronic myelogenous leukemia (CML) where the main cause of the disease is BCR-ABL fusion protein. This fusion protein is a kinase and has been reported to be effectively blocked by a drug named imatinib [2]. Similarly, another fusion protein named NUP98 has been identified in acute myeloid leukemia (AML) where it causes cancer through its interaction with CDK6, a cell division kinase [3].

A benzene ring and an azocine ring combine to form the chemical complex known as benzazocine [4]. In conventional chemotherapeutics, their compounds have reportedly emerged as a viable anticancer medication candidate. [5]. The title compounds (a) NAOP-12 (17-ethyl-9,16,20,27 tetraazahexacyclo [17.8.0.0^{2,7}.0^{8,16}.0^{10,15}.0^{21,26}] heptacosa-1(27),9,19-triene) (b) NEMKH-12 (17,18-dimethyl-9,16,20,27-tetraazahexacyclo [17.8.0.0^{2,7}.0^{8,16}.0^{10,15}.0^{21,26}] heptacosa-1(27),9,19-triene), which are novel benzazocine derivative, has been found to possesses anticarcinogenic activity against HCT 116, MCF 7, MDA-MB231 and HL 60 human cancer cell lines [6]. Density functional theory provides an accurate solution to the problem of electronic structure theory. The first stage of the DFT helps to make sense of the results of the spectrum evaluation. The material functioning of the title molecule can be predicted and calculated with the help of DFT simulations. This study produces some structural and biological properties of the compounds (a) and (b) using Gaussian 09 software by DFT/B3LYP method employing 6-311++G (d, p) basis set. The electronic descriptors like HOMO, LUMO, frontier orbital energy gap and molecular electrostatic potential surface (MESP) have been plotted to investigate the chemical reactivity of the molecules. Electrical parameters like dipole moment, molecular polarizability and first static hyperpolarizability, have been utilized to predict the biological nature and non-linear optical (NLO) behavior of the molecules. Fukui functions were calculated in terms of electron density, provides the information about reactive sites of the compounds, which were also predicted by their respective MESP plot. The Hirshfeld surface analysis was performed for the two compounds and fingerprint plots associated with them indicate the existence of some weak interactions. Structural stability of the protein-receptors and their affinity of binding to ligands NAOP-12 and NEMKH-12 has been studied using computational tools such as molecular dynamics simulation and gmxMMPBSA analyses. Molecular docking analysis has been performed by restricting our focus on molecules involved in anticarcinogenic activities. The ADMET and pharmacokinetic properties have also been calculated to investigate their pharmaceutical efficiency.

2. Material and Methods

The quantum chemical calculations of the title compounds (a) NAOP-12 and (b) NEMKH-12 were carried out using Gaussian 09 software [7]. In the present study, DFT has been incorporated using Becke's three parameters hybrid exchange functional B3LYP with Lee, Yang and Parr correlation functional [8-10]. The standard split-valence basis set 6-311++G (d, p) with (d) diffuse and (p) polarization functions, has been used in most of the calculations. Initially optimized geometry has been achieved, to calculate the vibrational frequencies, electric and electronic parameters, Fukui functions etc. The model molecular structures, HOMO-LUMO & MESP surfaces of the two compounds (a) and (b) are produced using Gaussian 5.0.8.2 program package [11]. ADMET and pharmacokinetic properties were calculated incorporating SWISSADME [12]. Gromacs 2024.4 software in the environment of Linux operating system platform was employed to perform entire molecular dynamics simulations [13]. The free energy for all the protein-ligands complexes were evaluated employing gmxMMPBSA tool [14]. The docking calculations were performed employing Autodock Vina tools 4.2.6 [15] and discovery studio.

3. Results and Discussion

3.1 Optimized Molecular Geometry

Molecular geometry generally shows the physical parameters in parallel to the constituents of a compound, through which the physical parameters can be explored. Both the title molecules contain an azocane ring R1, which is a saturated eight-membered ring, a diazine ring R2, an imidazole ring R4, three benzene rings R3, R5 and R6, resulting in the base compound as a benzazocine with analgesic activity. The equilibrium geometry optimization of lowest energy conformer has been achieved by energy minimization. The calculated vibration spectrum contains no imaginary wave number which indicates that optimized geometry of the two molecules NAOP-12 and NEMKH-12 are at minima on potential energy surface. The optimized structures of both the compounds are shown in fig. 1(a) and 1(b) respectively and they are very close to that obtained by X-ray diffraction analysis. The optimized bond lengths of (C-H) are within the range 0.93- 0.963 Å for Naop-12 and it was obtained in the range 1.08-1.10 Å for NEMKH-12. The (C-C) stretching is computed in the range 1.3632-1.4923 Å and 1.390-1.53 Å respectively for the two molecules. The intermolecular distances (C-N) are calculated in the range 1.318-1.435 Å and 1.32-1.36 Å respectively. These optimized bond lengths are in coherence with the experimental X-ray values as shown in tables T1(a) and T1(b) respectively. As a result, these geometrical data offer a reliable approximation when combined with experimental crystal data, and the results are appropriate for vibrational frequency calculations.

3.2 Vibrational Assignments

The examined compounds, NAOP-12 and NEMKH-12, have 44 and 47 atoms, respectively, and so display 126 and 135 normal vibrational modes. To study these vibrations, the vibrational modes are identified employing Gaussview 6.0,

and the potential energy distribution (PED) of these modes is computed employing VEDA 4.0 [16]. The an-harmonicity and the electron-electron interaction were disregarded [17]. The computed frequencies are in a higher range than the experimental values because of these approximations. As a result, we used 0.958 to scale the estimated frequencies up to 1700 cm^{-1} and 0.9688 for frequencies below that [18]. The experimental FTIR spectra of the two studied compounds are provided in supplementary information (SI) figures F1 and F2, and the corresponding simulated IR spectra plotted employing Gaussum 2.0 software are shown in figures (2a) and (2b) respectively. The explanations of a few significant vibrational modes are given below.

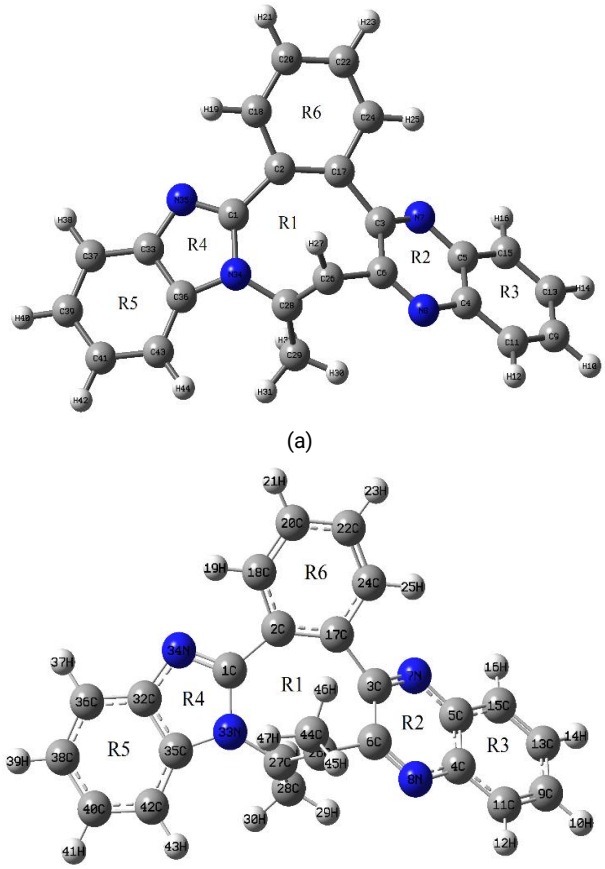

Fig. 1. Model molecular structure of (a) NAOP-12 and (b) NEMKH-12

3.2.1 C-H stretch

The v(C-H) vibrations of NAOP-12 are estimated in the frequency range 3092-3028 cm^{-1}. These vibrations appear as two modest absorption peaks at 3055 cm^{-1} and 3020 cm^{-1} in the FTIR spectra. Conversely, in NEMKH-12 these modes are within the 2800–3100 cm^{-1} range. The experimental values assign the three peaks at 3051, 2970, and 2922 cm^{-1} to these modes, which have high PED values. The C-H in plane bending frequencies is highly helpful for characterization and appears in the 1500–1000 cm^{-1} range. The computed frequencies accurately correspond to the C-H in plane bending vibrations, which show up as a prominent band in the FTIR spectra range 1526 to 1136 cm^{-1} and 1574 to 1122 cm^{-1} respectively.

3.2.2 C=C stretch

The v (C=C) stretching vibrations for NAOP-12 are calculated at 1651 and 1623 cm^{-1} and are assigned to a medium intense peak at 1686 cm^{-1} in FTIR spectrum, while for NEMKH-12 the calculated value is 1662 cm^{-1} and assigned to the experimental value at 1663 cm^{-1}, which is also a medium intense peak. These vibrational modes are in accordance with the reported literature [19].

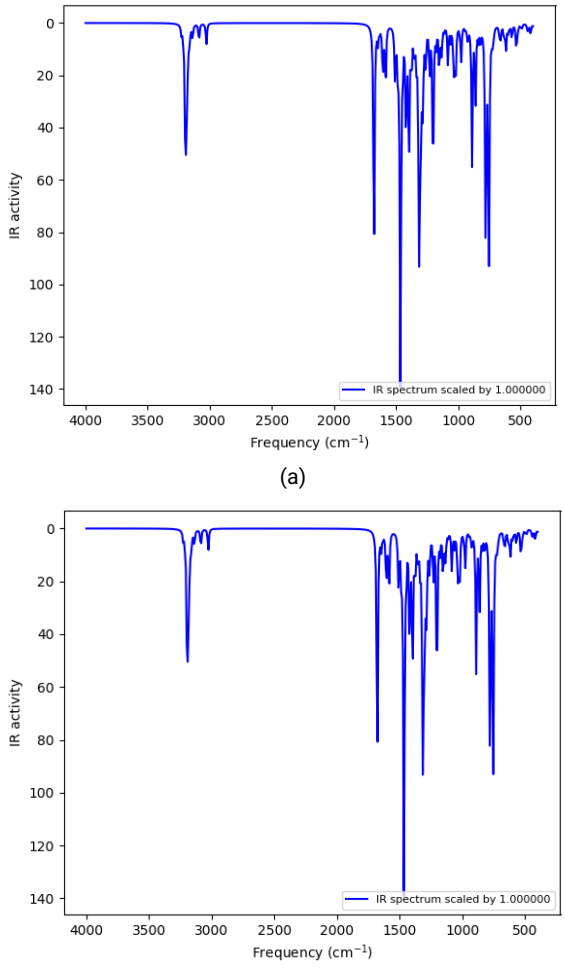

Fig. 2. Simulated IR spectrum of (a) NAOP-12 and (b) NEMKH-12.

3.2.3 C=N Stretch

For NAOP-12 this mode is computed at 1581 cm^{-1} and is assigned to a weak peak at 1605 cm^{-1} and for NEMKH-12 it was computed at the frequencies 1623 and 1619 cm^{-1} and is assigned to the experimental value at 1606 cm^{-1}, a medium strength peak.

3.2.4 C-C stretch

The v(C-C) aromatic stretch gives rise to the characteristic bands in the spectral range 1600-1000 cm^{-1} [19]. In the present study for NAOP-12, v(C-C) stretching vibrations are observed in FTIR spectra at frequencies 1606, 1557 and 1345 cm^{-1} which are calculated by DFT in frequency range 1606-1352 cm^{-1}, for NEMKH-12, these modes are calculated in the frequency range 1607-1322 cm^{-1} and are assigned to spectral values at 1606, 1533, 1445 and 1374 cm^{-1} and are mixed with the in-plane bending modes.

3.2.5 C-N stretch

The (C-N) vibrational modes are difficult to identify due to mixing with other vibrational modes in this region. The (C-N) stretching vibrations in NAOP-12 are allocated to the experimental frequency peaks in the spectrum at 1379, 1271, and 1238 cm^{-1} and are estimated in the frequency range 1375–1245 cm^{-1}. For NEMKH-12 (C-N) vibrational modes are observed to a significant peak at 1269 cm^{-1}, and they are computed in the frequency range 1315-1236 cm^{-1}. The literature supports these torsional, bending, and stretching modes [20].

3.2.6 Modes in the lower spectral region

Finding low-frequency vibrational modes is important because it sheds light on the weak intermolecular interactions that happen to take place during enzyme activities [21]. The interpretation of the impact of electromagnetic radiation on biological systems can also benefit from an understanding of low frequency modes [22]. Several torsional modes are seen in the lower-middle region of the experimental FTIR spectrum and are well matched with the computed values. The tables T2(a) and (b) include lists of each of these modes, respectively.

3.3 Frontier molecular orbital analysis

To comprehend the reactivity and area selectivity of diverse chemical systems, HOMO and LUMO have been utilized extensively. A molecule's softer and more unstable molecular structure is indicated by a narrower HOMO and LUMO gap, while a broader energy gap indicates a harder and more stable molecular structure. The soft molecules are generally unstable and chemically reactive [23, 24]. Fig. 3(a) and 3(b) represents the 2D plots of HOMO and LUMO of the two compounds respectively. Fig. 3(a) reveals that in NAOP-12, the entire HOMO is hovering over the imidazole ring R4, two benzene rings R5 and R6, and the pyrazine ring R2, and some portion of azocane ring R1 whereas LUMO is spread over the two benzene rings R2 and R3. As a result, the charge transfer occurs from the rings R4, R5, and R6 to rings R2, and R3. In the instance of NEMKH-12 in fig. 3(b), the HOMO distribution is the same, but in addition to rings R1, R2, and R3, a sizable quantity of LUMO is distributed over the benzene ring R6.

The computed HOMO-LUMO frontier energy gap for NEMKH-12 is less (3.69 eV) as compared to that of NAOP-12(3.82 eV) hence reactivity, and polarizability of NEKKH-12 is more; however, the stability of NAOP-12 is larger. In general, both the compounds possess high values of polarizability and chemical reactivity, therefore, belong to soft molecules [25, 26]. Molecular electrostatic plots (MESP) for the two compounds are presented in fig. 4(a) and 4(b) respectively. It is evident from these figures that azocine ring R1 is the least reactive site in both the compounds as it has got a minimum covered area with MESP; also, the region around the benzene ring R3 is electron deficient (minimum electrostatic potential shown with blue color) and have binding sites for nucleophilic attack. The electron rich region (maximum electrostatic potential shown with red color) is residing dominantly over the imidazole ring R5 and pyrazine ring R2 and hence are highly active centers for electrophilic attack.

Table 1 displays several computed electronic parameters which describes the overall reactivity of the compounds. For the molecules (a) and (b), the values of chemical softness are 0.2238 & 0.1849, chemical hardness as 1.9101 & 1.8450, electron affinity as 2.4192 & 2.4600, electronegativity as 4.3293 & 4.3050 and ionization potential as 6.2394 & 6.1500 respectively. These parameters along with the values of electrophilicity (4.9062 & 5.0225), suggest that both the compounds bear enough biological activities to test them further for medicinal purposes.

3.4 Fukui function and dual descriptors

The Mulliken atomic charges are obtained by DFT calculation of optimization of the title molecules (a) and (b) in three types, one by taking charge of the entire molecule as zero [q(N)], second as +1 [q(N+1)], and third as -1 [q(N-1)]. By using the Mulliken charges of the atoms of these compounds obtained in the above three optimization calculation, Fukui Functions (f_{k+},f_{k-},f_{k0}), are computed. Fukui function (FF) thus calculated in terms of electron density are used to get information about reactive sites of the molecule and in categorizing chemical reactions [27, 28]. The atom which gains highest FF value is highly reactive site as compared to the other atoms in the molecule. The local softness (S_{k+},S_{k-},S_{k0}) and local electrophilicity indices [ω_{k+},ω_{k-},ω_{k0})] are also calculated using the Mulliken atomic charges of neutral molecule q(N), cation [q (N+1)], and anion [q (N-1)], where +, - and 0 signs indicates nucleophilic, electrophilic and radical attacks respectively [29]. Fukui functions for the two title compounds (a) and (b) are presented in supplementary tables T3(a) and 3(b) respectively.

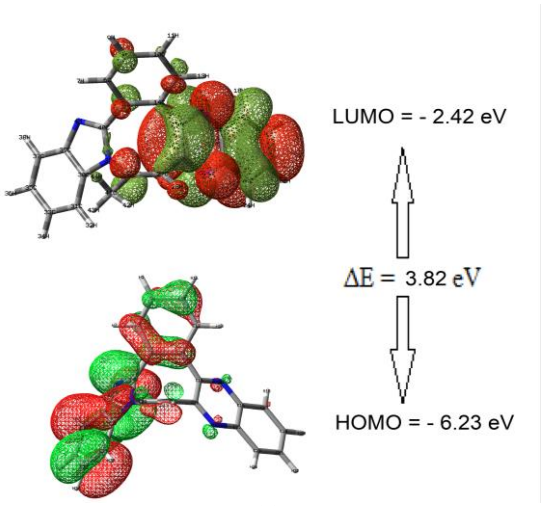

Fig. 3. 2D-HOMO-LUMO plot of (a) NAOP-12 and (b) NEMKH-12.

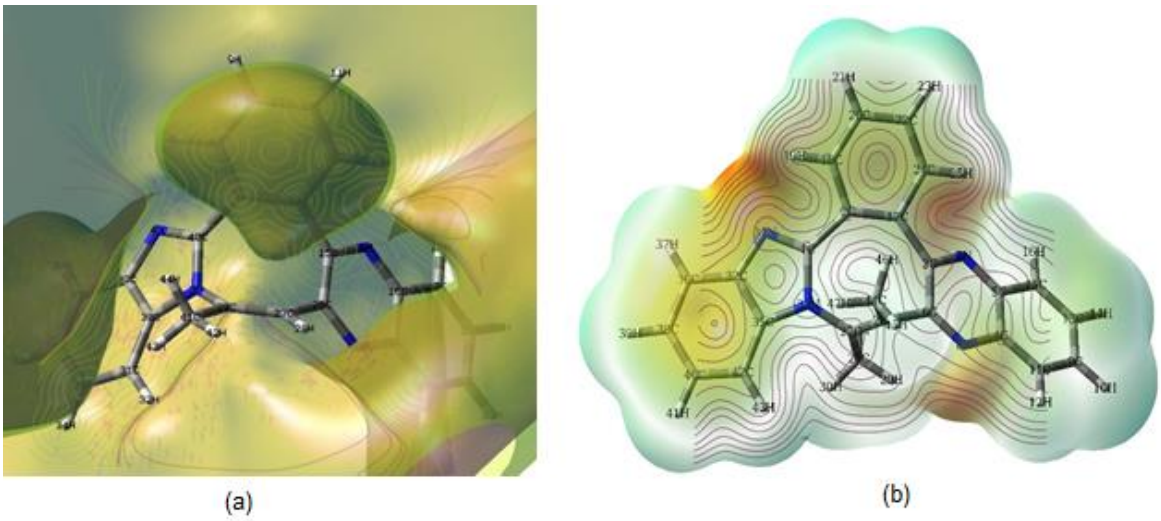

Fig. 4. 2D MESP plot of (a) NAOP-12 and (b) NEMKH-12.

Table 1. Electronic parameters of (a) NAOP-12 and (b) NEMKH-12

Parameters	DFT-Values	
	NAOP-12	NEMKH-12
E_{HOMO} (eV)	-6.2394	-6.1500
E_{LUMO} (eV)	-2.4192	-2.4600
ΔE (eV)	3.8202	3.6900
Ionization potential (I)	6.2394	6.1500
Electron affinity(A)	2.4192	2.4600
Electronegativity(χ)	4.3293	4.3050
Chemical potential(μ)	-4.3293	-4.3050
Chemical hardness(η)	1.9101	1.8450
Global softness(S)	0.2618	0.2710
Electrophilicity index (ω)	4.9062	5.0225
Fukui function(fk+-)(max value)	0.8550	0.6823
Local softness (S*fk+-)	0.2238	0.1849
Electrophilicity (ω*fk+-)	4.1946	3.4269

For the compound (a), atoms 28C, 1C, 6C and 20C are favorable sites for both electrophilic and nucleophilic attack. The atom 28C is the most reactive site for radical attack (0.3188) and has got maximum value of local softness (0.2238). Therefore carbon atom 28C is most reactive in nature. Table 3(b) shows that for the compound (b), most nucleophilic attack prone site is the atom 27C, whereas most electrophilic reactive attacking sites is the atom 44C. The hydrogen atom 19H is the most reactive site for radical attack. The local softness has got maximum value at the atomic site 27C (0.1342). The dual descriptor method is more accurate than Fukui function, and its computed values are also displayed in the tables.

3.5 Electrical and Non-Linear Optical parameters

Nonlinear optics plays vital role in telecommunications, signal processing, and interconnections, such as frequency switching, optical modulation, optical switching, optical logic, and optical memory [30]. Dipole moments for molecules (a) and (b) are found to be along the X-Z plane, with computed values of 1.8521 D and 2.49 D, respectively. This suggests that molecule (b) has a greater capacity to transmit charges. The component α_{ZZ} contributes more to the mean polarizability <α> in both compounds than do components α_{XX} and α_{YY}, which is why they are more elongated along the Z-axis. The mean polarizability <α> was calculated to be -154.223 and -161.18 a.u. respectively, these polarizability values suggests that both the compounds NAOP-12 and NEMKH-12 may exhibit considerable number of biological activities. Table 2 shows some relevant electric parameters like dipole moment, polarizability, and first-order hyperpolarizability for the two title molecules. Because of the hydrogen bond interaction, organic compounds containing (N-H) group exhibit increased molecular hyperpolarizability and mechanical stabilities. The first order hyperpolarizability can also be connected to the band gap of energy between the HOMO and LUMO. So, the higher the band–gap is, the lower the first hyperpolarizability.

The NEMKH-12 has got lesser computed band gap (3.69 eV) and therefore has got higher β_{tot} as compared to NAOP-12. The value of first-order hyperpolarizability β_{tot} for NAOP-12 and for NEMKH-12 are computed as 0.713×10^{-30} e.s.u. and 0.8609×10^{-30} e.s.u. respectively, both are more than double to that of benchmark compound Urea (β_{tot} =0.3728×10^{-30} e.s.u) hence they have considerable potential to treat as NLO materials [31, 32].

3.6 Drug Likeness & ADME profiles

ADME profiles and drug likeness parameters were calculated using PreADME and SWISSADME online software respectively for both the title compounds and are summarized in table 3. Lipinski rule of 5 (LiR of 5), helps in distinguishing between drug like and non-drug like molecules. The calculated values of drug likeness parameters for the compounds (a) and (b) are (i) HBD is 0 (≤5) (ii) HBA as 3 and 4 (≤10), (iii) MW as 380.57 & 394.6 g/mol (≤500 g/mol), (iv) MR as 132.64 &

137.45 (40<MR<130), (v) log P as 3.88 & 4.23 respectively, showing excellent permeability across biological membranes and good binding to plasma proteins for both molecules [33-35]. The values of van der Waals topological polar surface area (TPSA) are 40.32 Å^2 (<120 Å^2), partition coefficient (Milog P) is calculated as 3.88 &4.23 (≤5) respectively. Therefore, it is evident that both the molecules have passed the LiR of 5 and thus are qualified to be tested in vivo.

Table 2. Electrical parameters of NAOP-12 & NEMKH-12. (1 a.u.=8.3693*10^{-33} e.s.u).

Polarizability	Values(a.u)		Hyperpolarizability	Values(a.u)	
	NAOP-12	NEMKH-12		NAOP-12	NEMKH-12
α_{XX}	146.0344	-154.28	β_{XXX}	72.1256	90.74
α_{XY}	-2.4336	2.17	β_{XXY}	50.2276	-47.87
α_{YY}	148.7629	-157.72	β_{XYY}	5.5473	-4.14
α_{YZ}	-3.6188	-3.86	β_{YYY}	30.4097	33.97
α_{ZZ}	167.8705	3.08	β_{XXZ}	39.1538	-35.55
α_{XZ}	-3.9554	-171.55	β_{XYZ}	-1.1446	-4.34
<α>	-154.223	-161.18	β_{YYZ}	10.4088	7.03
Dipole Moment (1 Debye= 3.3356 x 10^{-30} Col-m)			β_{XZZ}	-9.8816	13.01
			β_{YZZ}	1.1201	-3.08
μ	1.8521	2.491	β_{ZZZ}	3.9709	9.20
			β_{Total}	85.2412	102.87

In ADME parameters, human intestinal absorption (HIA) results are the sum of absorption and bioavailability determined from collective excretion in urine, bile, and feces [36, 37]. The HIA values are calculated as 98.17% and 98.20% respectively. CaCo-2 is a human colon epithelial cell line that is frequently used as a model system for assessing the absorption of drugs by the human digestive tract and the values are calculated as 24.065 & 24.286 which are in permissible range and hence, possess excellent intestinal absorption. Madin Darby Canine Kidney (MDCK) cells are very important for determining the fast permeability of drug molecule because the growth period of MDCK cells is shorter than CaCo-2 cells [38]. The MDCK cell permeability values are calculated as 58.323 & 51.734 nm/s respectively, which are sufficient for clearance through the renal cells. The skin permeability computed negative values (-2.74 & -2.57) for the compounds exhibit that they do not possess any skin permeability effect.

Plasma protein binding are calculated as 96.127 and 96.814 respectively showing excellent bioavailability. The ability of both the molecules NAOP-12 and NEMKH-12 to inhibit CYP3A4, CYP2C9 and CYP2C19 shows that the molecules don't require xenobiotic metabolism in the body. There is no rotatable bond for both the compounds. For both in vitro and in silico evaluations of drug-like qualities, the predicted pharmacokinetic parameters and physicochemical features known as Lipinski's filters are essential [39, 40]. In the latter stages of drug development, a molecule with poor pharmacokinetic qualities and noncompliance with Lipinski's filters fails.

Table 3. Drug Likeness, ADME parameters of NAOP-12 & NEMKH-12

S.No	Drug Likeness parameters			S.No.	ADME parameters		
	Parameters	NAOP-12	NEMKH-12		Parameters	NAOP-12	NEMKH-12
1	Formula	C24H16N4	C25H18N4	15	GI absorption	High	High
2	MW	380.57	394.6	16	BBB permeant penetration (c.brain/ c.blood)	6.90649	6.25979
3	Rotatable bonds	0	0	17	Caco-2 cell permeability (nm/s)	24.0654	24.2861
4	Heavy atoms	28	29	19	CYP_2C9_inhibition	Inhibitor	Inhibitor
5	Aromatic heavy atoms	0	0	20	CYP_2D6_inhibition	Non	Non
6	Fraction Csp3	0.88	0.88	21	CYP_2D6_substrate	Non	Non
7	H-bond acceptors	3	4	22	CYP_3A4_inhibition	Inhibitor	Inhibitor
8	H-bond donors	0	0	23	CYP_3A4_substrate	Weakly	Weakly
9	MR	132.64	137.45	24	HIA (%)	98.17154	98.204734
10	TPSA	40.32	40.32	25	MDCK cell permeability (nm/s)	58.3237	51.7347
11	iLOGP	3.88	4.23	26	Pgp_inhibition	Inhibitor	Inhibitor
12	MLOGP	3.67	3.88	27	Plasma_Protein_Binding	96.12767	96.814922
13	ESOL Log S	-3.83	-4.48	28	Pure_water_solubility_mg_L	0.621238	0.153737
14	Ali Log S	-3.09	-4.01	29	Skin_Permeability	-2.73552	-2.56909

3.6.1.Toxicity predictions

Analysis of toxicity plays an important role in drug development and helps identify adverse effects of new drugs on the body. The toxicity of both the compounds were calculated using ProTox-II online software [41]. Organ toxicity results suggested that both the compounds were predicted to be hepatotoxic, neurotoxic and respiratory toxic. The toxicity end-points results predicted that these compounds had shown immunotoxicity and ecotoxicity and are inactive for blood-brain-barrier. The CNS active molecules always penetrate Blood–Brain Barrier (BBB) and cause collateral effects in CNS [42, 43]. Both the ligands are inactive for molecular initiative events for most of the parameters including GABA receptor. All the toxicity parameters are given

in the table 4 and it was concluded that both the compounds exhibited the same toxicity behaviour.

Table 4. Insilco toxicity evaluation of the compounds.

Toxicity		NAOP-12		NEMKH-12	
		Activity	Probability	Activity	Probability
Organ Toxicity	Hepatotoxicity	Active (+)	0.69	Active	0.69
	Neurotoxicity	Active(+)	0.87	Active	0.87
	Nephrotoxicity	Inactive(-)	0.90	Inactive	0.90
	Respiratory toxicity	Active(+)	0.98	Active	0.98
	Cardiotoxicity	Inactive(-)	0.77	Inactive	0.77
	Carcinogenicity	Inactive(-)	0.62	Inactive	0.62
	Immunotoxicity	Active(+)	0.96	Active	0.96
Toxicity end points	Mutagenicity	Inactive(-)	0.97	Inactive	0.97
	Cytotoxicity	Inactive(-)	0.93	Inactive	0.93
	BBB-barrier	Inactive(-)	1	Inactive	1
	Ecotoxicity	Active(+)	0.73	Active	0.73
	Clinical toxicity	Inactive(-)	0.56	Inactive	0.56
	Nutritional toxicity	Inactive(-)	0.74	Inactive	0.74
Tox21-Nuclear receptor signalling pathways	Aryl hydrocarbon Receptor (AhR)	Inactive(-)	0.97	Inactive	0.97
	Androgen Receptor (AR)	Inactive(-)	0.99	Inactive	0.99
	Androgen Receptor Ligand Binding Domain (AR-LBD)	Inactive(-)	0.99	Inactive	0.99
	Aromatase	Active(+)	1	Active	1
	Estrogen Receptor Alpha (ER)	Active(+)	0.99	Active	0.99
	Estrogen Receptor Ligand Binding Domain (ER-LBD)	Active(+)	1	Active	1
	Peroxisome Proliferator Activated Receptor Gamma (PPAR-Gamma)	Inactive(-)	0.99	Inactive	0.99
Tox21-Stress response pathways	Nuclear factor (erythroid-derived 2)-like 2/antioxidant responsive element (nrf2/ARE)	Inactive	0.88	Inactive	0.88
	Heat shock factor response element (HSE)	Inactive	0.88	Inactive	0.88
	Mitochondrial Membrane Potential (MMP)	Inactive	0.70	Inactive	0.70
	Phosphoprotein (Tumor Supressor) p53	Inactive	0.96	Inactive	0.96
	ATPase family AAA domain-containing protein 5 (ATAD5)	Inactive	0.99	Inactive	0.99
Molecular Initiating events	Thyroid hormone receptor alpha (THRα)	Inactive	0.90	Inactive	0.90
	Thyroid hormone receptor beta (THRβ)	Inactive	0.78	Inactive	0.78
	Transtyretrin (TTR)	Inactive	0.97	Inactive	0.97
	Ryanodine receptor (RYR)	Inactive	0.98	Inactive	0.98
	GABA receptor (GABAR)	Inactive	0.96	Inactive	0.96
	Glutamate N-methyl-D-aspartate receptor (NMDAR)	Inactive	0.92	Inactive	0.92
	alpha-amino-3-hydroxy-5-methyl-4-isoxazolepropionate receptor (AMPAR)	Inactive	0.97	Inactive	0.97
	Kainate receptor (KAR)	Inactive	0.99	Inactive	0.99
	Achetylcholinesterase (AChE)	Active	0.69	Active	0.69
	Constitutive androstane receptor (CAR)	Inactive	0.98	Inactive	0.98
	Pregnane X receptor (PXR)	Inactive	0.92	Inactive	0.92
	NADH-quinone oxidoreductase (NADHOX)	Inactive	0.97	Inactive	0.97
	Voltage gated sodium channel (VGSC)	Inactive	0.95	Inactive	0.95
	Na+/I- symporter (NIS)	Inactive	0.98	Inactive	0.98

3.7 Hirshfeld surface analysis

Hirshfeld surface depicting weak intermolecular interactions present in the crystal structure is plotted over d_{norm} for NAOP-12 and NEMKH-12 employing crystal structure file (cif) as input, are presented in fig. 5(a) and fig. 5(b) respectively. The Crystal Explorer 21 package is used to compute Hirshfeld surface and 2D fingerprint plots [44]. It is evident that both molecules (a) and (b) consists of two dominant weak interactions viz. C-H…N, C-N…H and N-C…H, N-H…C, with neighboring molecules indicated with red spots over the d_{norm} surface. The distance between these interactions is also mentioned on the 2D plots. In order to gain a better understanding of the weak interactions, 2D fingerprint representations of the two compounds have been plotted; these are presented in fig. 6 and fig. 7, respectively. They demonstrate the contributions of the individual N-H/H-N and C-H/H-C interactions to the overall interactions.

For NAOP-12, important interactions are C---H (17.8%)/ H--C (13.8%) to a total of 31.7% of H---C interactions are shown by two sharp peaks in fig. 6 (a, b, c); and the other important contributions are N----H (8.3%)/H---N (6.8%) contacts corresponding to total N---H (15.2%) interactions are shown by two sharp spikes fig.6 (d, e, f).

For NEMKH-12, values for the corresponding interactions are C---H (20.7%)/ H---C (16.3%) to a total of 37% of H---C interactions and are shown by two sharp peaks in Fig. 7 (a, b, c); and the other interactions are N---H (8.6%)/H---N (7.2%) contacts corresponding to total N---H (15.8%) interactions are shown by two sharp spikes in Fig.7 (d, e and f). It is clear that the weak interaction of H-bonding is a bit larger in the compound NEMKH-12 as compared to NAOP-12. The sharp peaks in the fingerprint plots indicating the presence of strong H-bonding interactions.

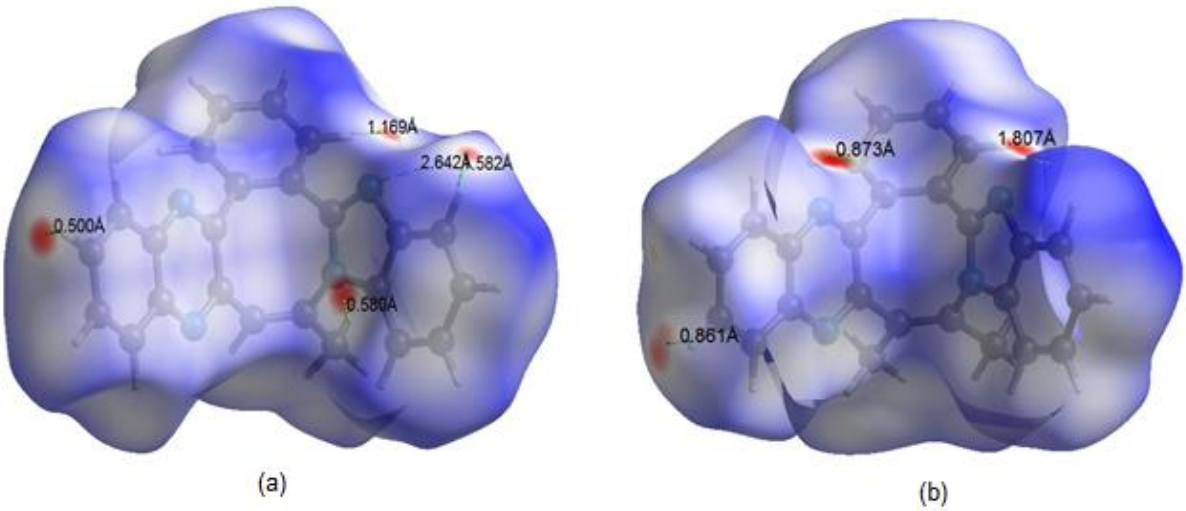

Fig. 5. 2D plot of crystal surface of (a) NAOP-12 and (b) NEMKH-12.

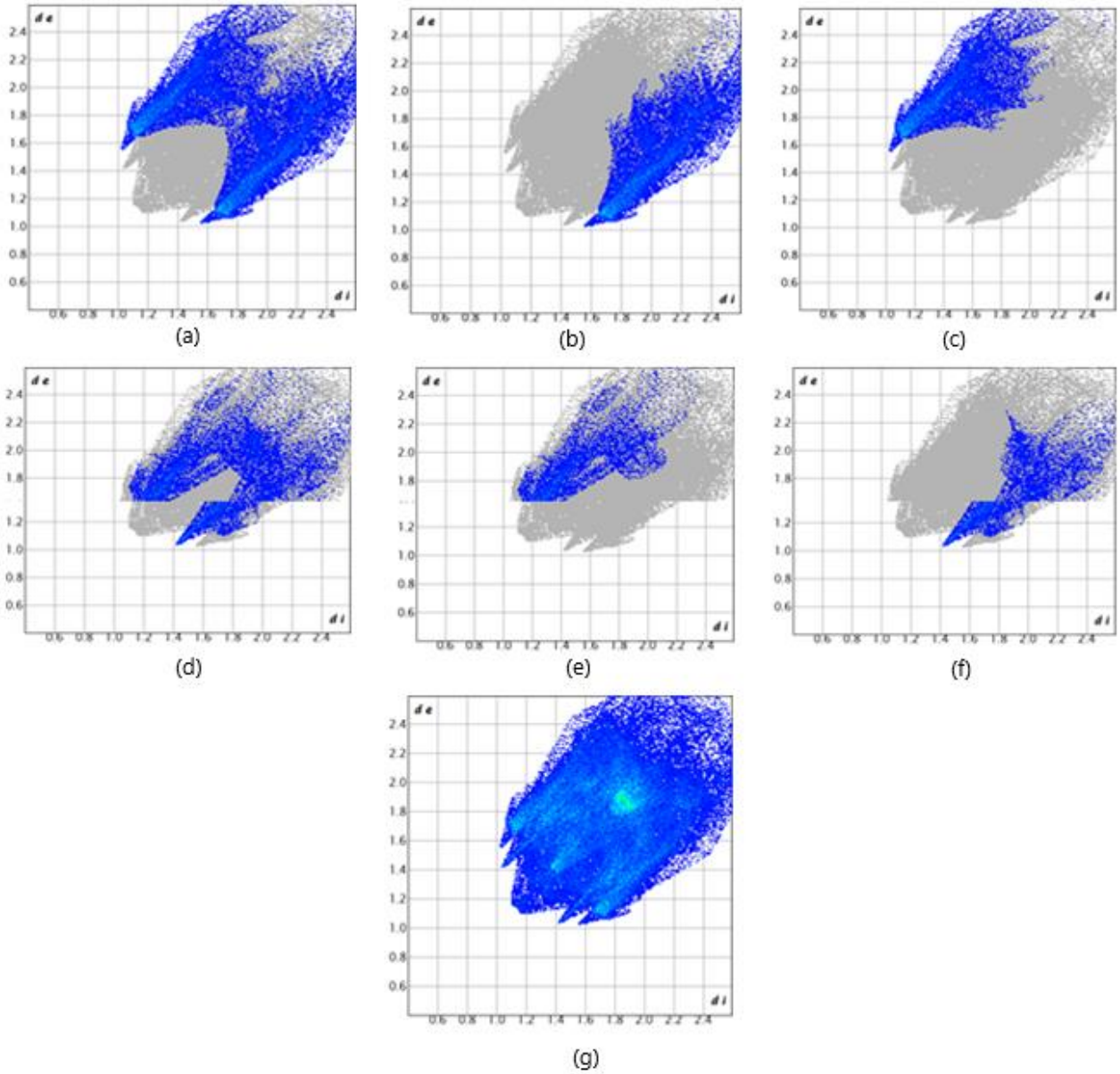

Fig. 6. (a) Total H—C, (b) C—H, (c) H—C, (d) Total H—N, (e) H—N, (f) N—H, (g) All interactions of NAOP-12.

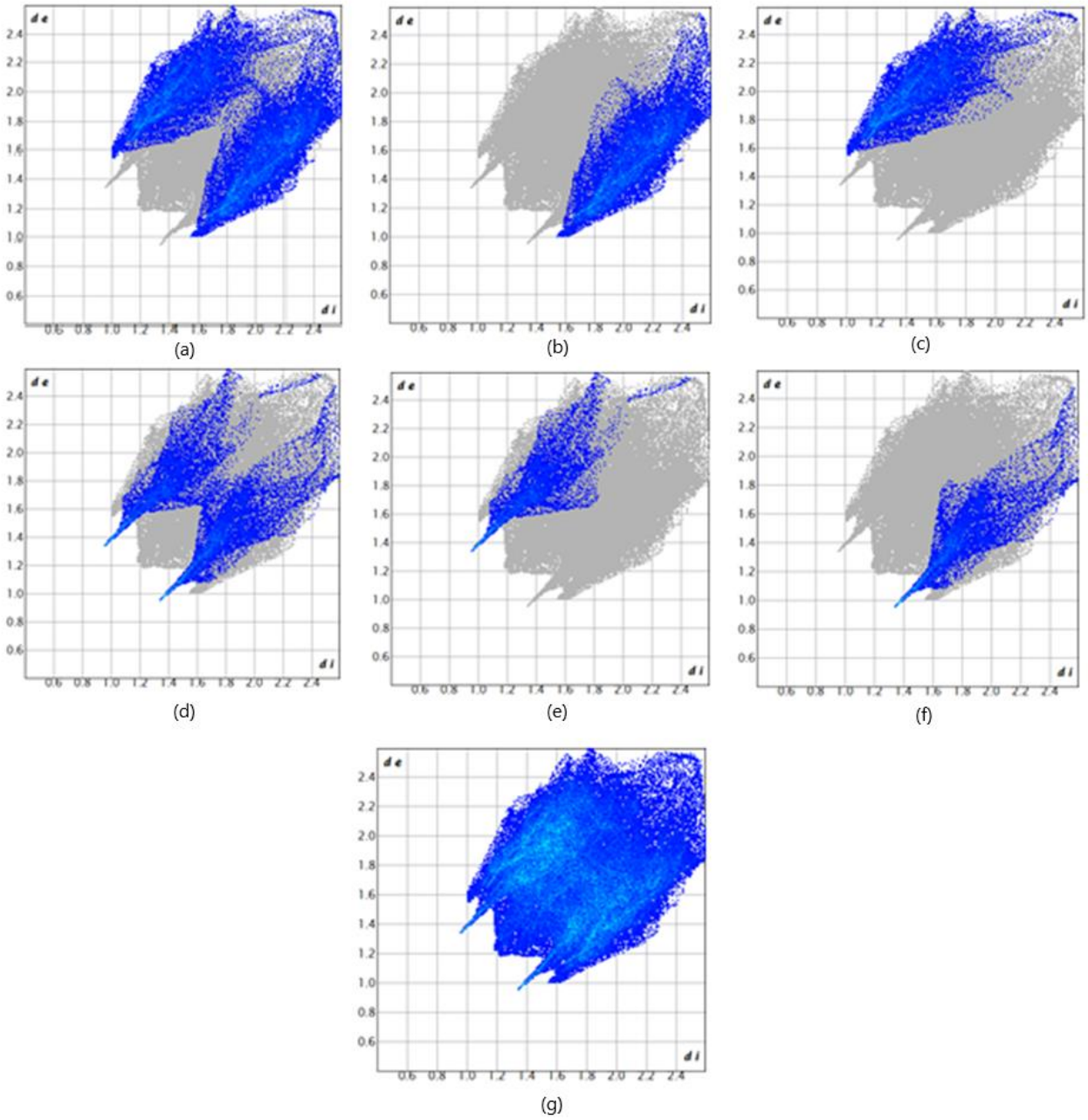

Fig. 7. (a) Total H—C, (b) C—H, (c) H—C, (d) Total H—N, (e) H—N, (f) N—H, (g) All interactions of NEMKH-12.

3.8 Molecular Dynamics Simulations

3.8.1 RMSD Analysis

The structural behaviour of ligands in the active region of proteins was investigated using the root mean square deviation (RMSD) technique. The RMSD plots of the two investigated ligands, NAOP-12 (green) and NEMKH-12 (red), with the protein receptor 6J7A are shown in figure 8(a). For NAOP-12, initially, it bounces between σ = 0.1 and 0.2 nm and after 100 ns, it climbs to 0.5 nm and then swings between 0.4 and 0.58 nm before stabilizing at 0.45 nm close to 500 ns. For NEMKH-12 the RMSD fluctuates between 0.2 and 0.3 nm before stabilizing at σ = 0.2 nm.

The final stabilized values of various parameters calculated during molecular dynamics simulations have been listed in table 5. The change in total binding free energies ΔG_{total} for all the protein-ligand combinations has got less than -7 Kcal/mol and the therefore they all have strong binding affinities.

Table 5. Stabilized parameters of molecular dynamics simulations.

Ligand-Protein complex	ΔGtotal Kcal/mol)	RMSD (nm)	RMSF(nm)	R_g(nm)	SASA(nm^2)	H-bonds
6J7A_NAOP-12	-11.22	0.45	0.13	2.93	375	1
65J7A_NEMKH-12	-18.89	0.2	0.125	2.91	390	1
6J7I_NAOP-12	-8.41	0.45	0.125	2.935	395	1
6J7I_NEMKH-12	-17.51	0.15	0.15	2.925	385	1

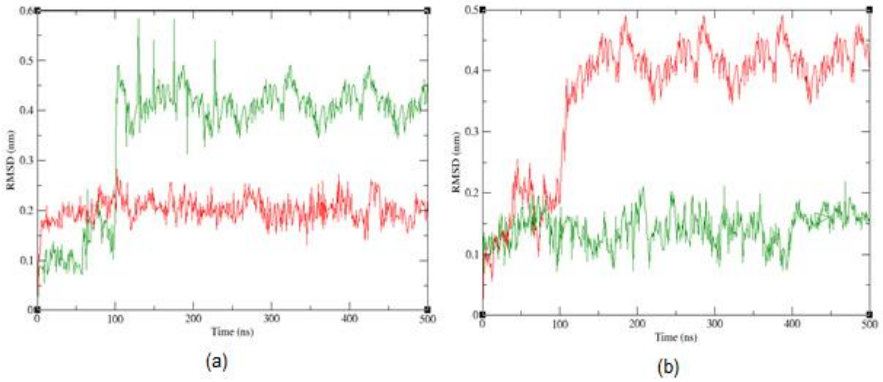

Fig. 8. RMSD fluctuations of two ligands NAOP-12 (green) and NEMKH-12 (red) with proteins (a) 6J7A and (b) 6J7I.

The situation is reversed for the other protein receptor, where RMSD (σ) is stabilized at 0.45 for NEMKH-12 and 0.15 for NAOP, as demonstrated in figure 8(b).

The root mean square (RMS) fluctuations of the two title molecules with the two receptor proteins, 6J7A and 6J7I, respectively, are shown in figures 9(a) and 9(b).

3.8.2 Root Mean Square Fluctuations

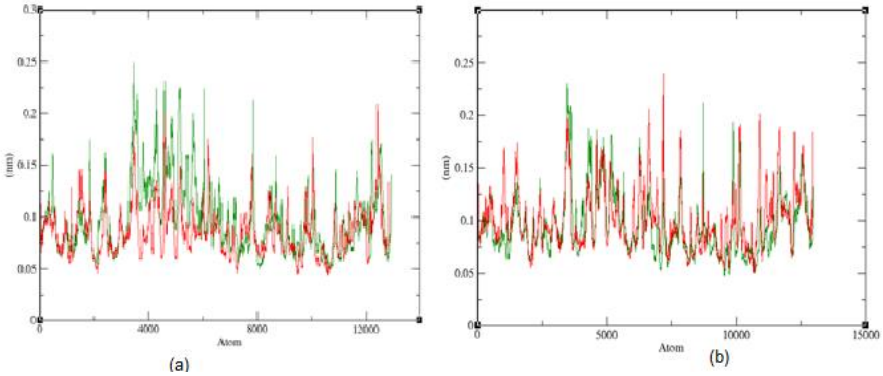

Fig. 9. RMS fluctuations of the ligands NAOP-12 (green) and NEMKH-12 (red) with the proteins (a) 6J7A and (b) 6J7I.

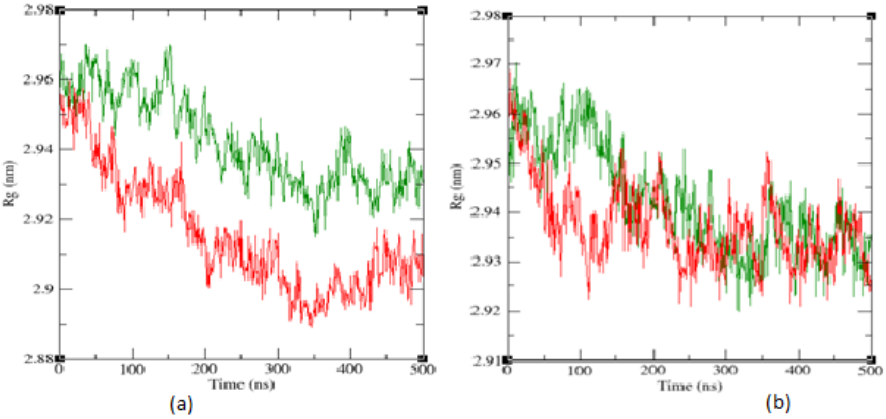

Fig. 10. Radius of gyration Rg of the ligands NAOP-12 (green) and NEMKH-12 (red) with the proteins (a) 6J7A and (b) 6J7I.

According to the comparative data, the RMS fluctuations are greatest between the proteins 3500-8000 atoms, with values of 0.25 and 0.225, respectively. It is clear that both ligands affected the structural behaviour of the two protein receptors and contributed equally to their RMS fluctuations.

3.8.3 Radius of Gyration (R_g)

The radius of gyration (R_g) can be used to determine the amount of rigidity of a protein structure. During the 100 ns simulation period, proteins that are folded steadily, display values that are comparatively constant, whereas proteins that are misfolded or unstable, exhibit fluctuations. The 2D plot in figure 10(a) shows that following early fluctuations, the R_g values of 6J7A are stabilized at 2.91 nm by NAOP-12 and at 2.93 nm by NEMKH-12. The trend is the same for the protein 6j7i (figure 10b), with the exception that R_g values for NAOP-12 and NEMKH-12 are stabilized at 2.935 and 2.925 nm, respectively.

3.8.4. Solvent-Accessible Surface Area (SASA)

The graphical depictions of the SASAs are shown in figures 11(a) and 11(b). It is evident that for the receptor protein 6J7A the values of Solvent Accessible Surface Area (SASA) for two ligands NAOP-12 and NEMKH-12 fluctuates around 380 to 390 nm^2 till 200 ns and are settled at 375 and 390 nm^2.

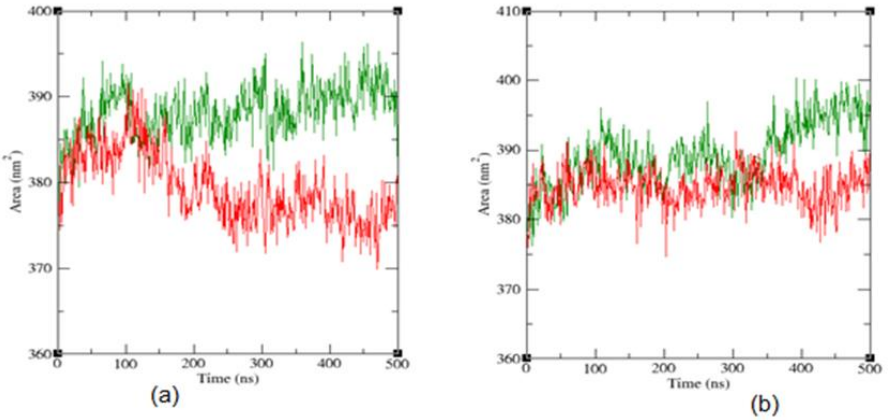

Fig. 11. Solvent accessible surface area (SASA) of the ligands NAOP-12 (green) and NEMKH-12 (red) with the proteins (a) 6J7A and (b) 6J7I.

For the receptor 6J7I SASA for both the ligands fluctuates between 380 to 390 nm^2 till 350 ns and stabilized at 395 and 385 nm^2 respectively. The higher SASA value of both the protean receptors indicates the large area was accessible to the solvent and hence the instability.

Figure 12(a) displays the number of H-bonds formed between ligands NAOP-12 and NEMKH-12 with the protein 6J7A and similarly figure 11(b) for protein 6J7I during entire simulation. It is obtained that NEMKH-12 forms larger number of hydrogen bonds in the vicinity of 0.34 nm distance, thus is more soluble and more viscous as compared to NAOP-12.

3.8.5 Hydrogen bonds

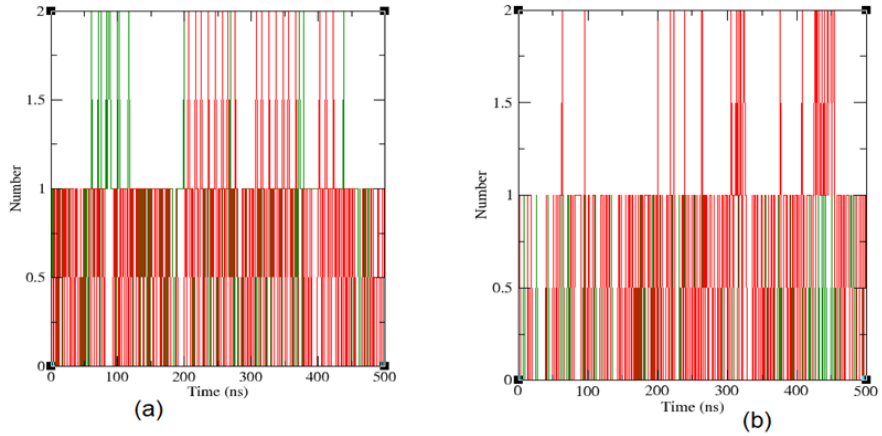

Fig. 12. Hydrogen bonds of the ligands NAOP-12 (green) and NEMKH-12 (red) with the proteins (a) 6J7A and (b) 6J7I.

3.8.6 PC1 and PC2 projections

Two-dimensional projections of PC1 and PC2 throughout the course of MD simulations for the two ligands with the two proteins 6J7A and 6J7I are presented in the figures 13(a) and 13(b) respectively. It is observed that in first protein 6J7A the projection of NAOP-12 is larger than NEMKH-12 whereas for 6j7i protein the case is reverse.

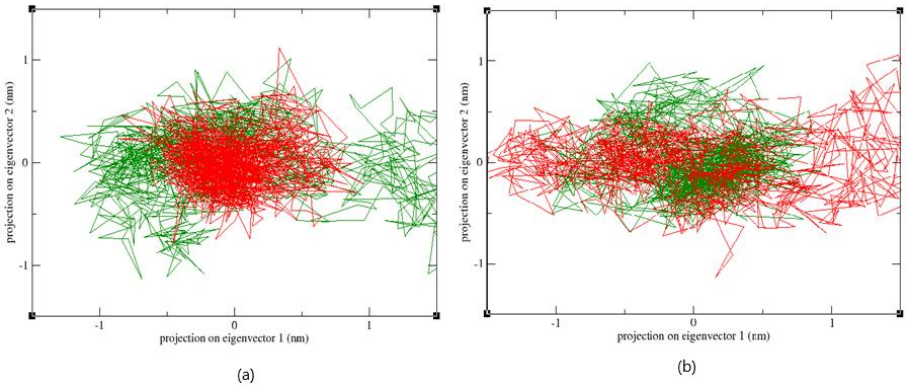

Fig. 13. 2D-Projection's trajectories PC1 and PC2 of the ligands NAOP-12 (green) and NEMKH-12 (red) with the protein receptors (a) 6J7A and (b) 6J7I.

3.8.7 gmxMMPBSA analysis

The binding free energy for the four protein-ligand combinations were calculated employing molecular mechanics/Poisson-Boltzmann surface area (mmPBSA). It has been reported that this technique balances precision with computational effectiveness, particularly when working with big systems [14]. Therefore, free energy calculation was carried out using the gmxMMPBSA tool, utilizing Gromacs trajectory and topology files. An index file was generated at the start and the output was saved in DAT (.dat) and CSV (.csv) format. All the energetic components along with the total change in binding energy during the course of simulations were captured using gmxMMPBSA ana module and is represented in figure 15(a-d).

3.9 Molecular Docking

For docking analysis, the probable target proteins (PDB ID: "6J7A" & "6J7I") have been predicted using online Swiss target prediction tool. The target proteins have been obtained from Protein Data Bank [45]. The selected proteins receptor were fusion proteins of heme oxygenase-1 and NADPH cytochrome P450 reductase CYPOR which are involved in NADPH-dependent electron transport pathway to oxidize a variety of physiological processes like drug metabolism, steroid biosynthesis, and bioactive metabolite production.

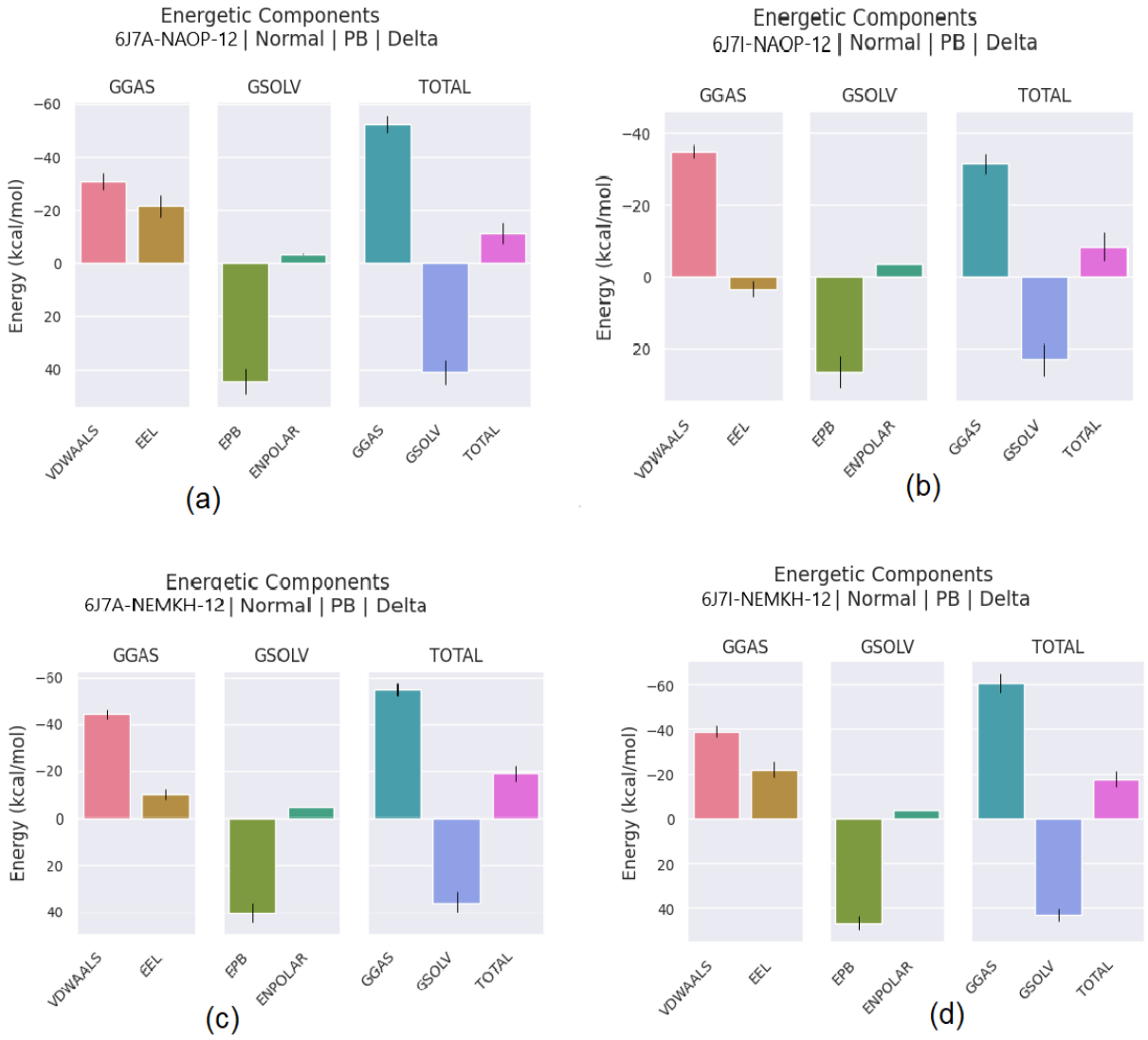

Fig. 14. Free energy values employing the gmxMMPBSA toll for the four protein-ligand complexes.

The ligands, proteins and grid maps were prepared for docking utilizing Auto Grid, and Auto dock tools whereas docking calculations were performed using the Autodock Vina 4.2.6 software [15].

2D interactions profile images of ligands NAOP-12 and NEMKH-12 with proteins 6J7A and 6J7I have been prepared using PYMOL software [47]. For the NAOP-12 and 6J7A protein receptor the interacting polar bond was observed with residue LYS-179 at 4.0 Å bond length and interaction energy -9.5 Kcal/mol (fig. 15a). For the NAOP-12 and 6J7I protein receptor complex the interacting polar bond was observed with residue ALU-824 at 4.3 Å bond distance and -10.5 Kcal/mol interaction energy (fig. 15b). For the protein 6J7A and ligand NEMKH-12 combination the interacting residue was TYR-357 at bond length 2.7 Å and -9.7 Kcal/mol interaction energy (fig. 15c).

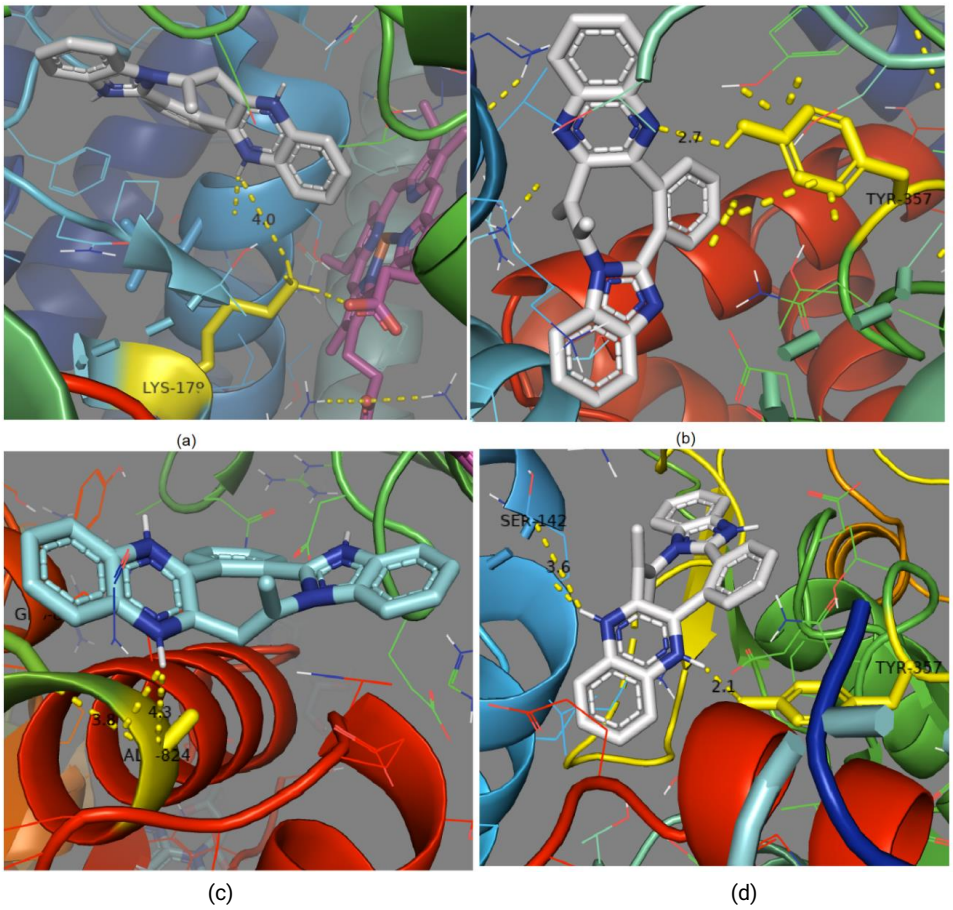

Fig. 15. 2D-poses of molecular docking of four protein-ligand complexes (a) 6J7A-NAOP-12. (b) 67JA-NEMKH-12. (c) 6J7I-NAOP-12 and (d) 6J7I-NEMKH-12 showing interacting residues with distances.

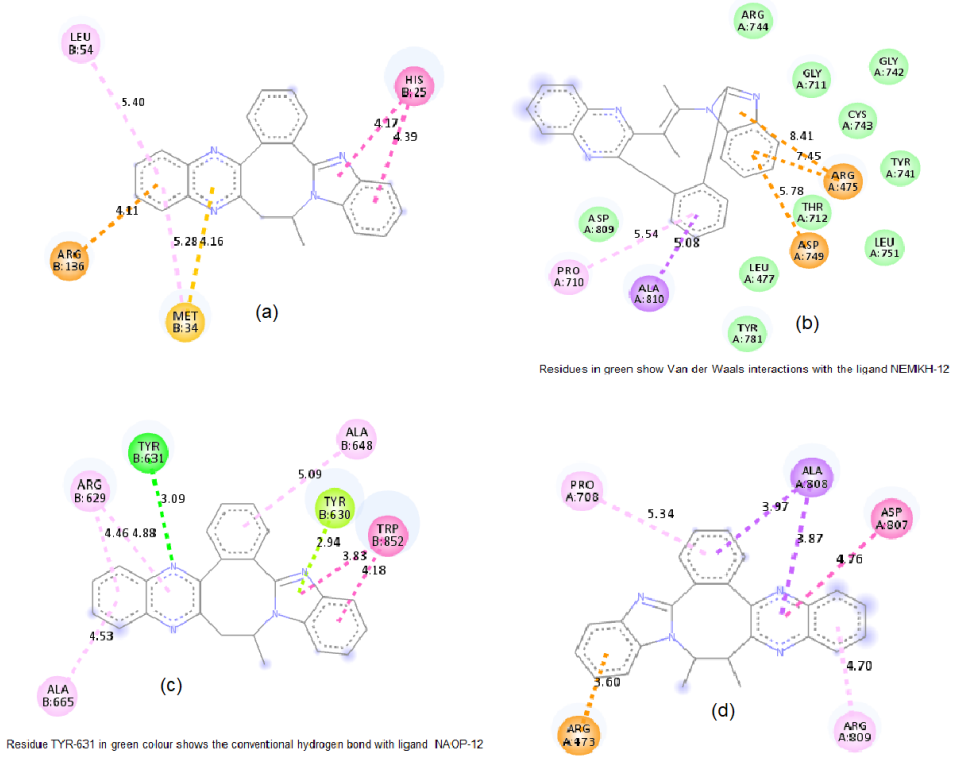

Fig. 16. 2D docking postures for the four protein ligand complexes (a) 6J7A-NAOP-12. (b) 6J7A-NEMKH-12. 9c) 6J71-NAOP-12 and (d) 6J7I-NEMKH-12 employing discovery studio visualizer.

Two interacting residues namely TYR-357 at bond length 2.1 Å and SER-142 at 3.6 Å, of protein 6J7I with NEMKH-12 were observed with -10.8 Kcal/mol interaction energy (fig. 15d). The 2D docking postures were also sketched using discovery studio visualizer and the interactions via CH with the protein residues of the title ligand molecules were identified in figures 16(a-d) as hydrogen bond and Van Der Waals interactions [48, 49].

4. Conclusions

This paper reports a comprehensive theoretical quantum chemical study on two benzazocine compounds NAOP-12 and NEMKH-12 for the first time. The molecular geometry, vibrational frequency, infrared intensities, NLO behavior and Fukui functions of the molecules have been calculated using DFT (B3LYP) method adopting 6-311++G(d,p) basis set. A good agreement between experimental and calculated normal modes of vibrations was achieved. The nonlinear optical (NLO) behavior of the molecules had been observed by the electric descriptors and it was concluded that both the compounds have enough favorable NLO properties. HOMO-LUMO plot, and low frontier energy gaps of the title compounds (3.82 and 3.69 eV) reveal their strong polarizability and chemical reactivity. The electrophilicity values, (4.9062, 5.0225) for the two compounds suggested about their excellent biological activities.

Fukui functions suggest that the carbon atom 28C is highly reactive in nature for electrophilic, nucleophilic, radical attack in NAOP-12 whereas it is 27C, 44C and 19H for NEMKH-12 respectively. Hirshfeld surface analysis revealed that there are sharp peaks in the fingerprint plots indicating the presence of H-bonding interactions which has also been obtained in the molecular dynamics.

Results of molecular dynamics simulations revealed that ligand NEMKH-12 had got lesser values of binding free energy, RMSD, RMSF and R_g parameters as compared to the second ligand NAOP-12. Results of molecular docking between title ligands (a) NAOP-12 and (b) NEMKH-12 with proteins 6J7A and 6J7I reveal that NEMKH-12 and protein 6J7I have got the tightest docking with interaction energy -10.8 Kcal/mol which is supported by molecular dynamics results. The duo compounds demonstrated favorable ADMET properties and also satisfied Lipinski's drug similarity filters. These results should pave the way for the synthesis of further novel biologically active compounds with imidazole and benzazocine rings. Our results corroborate with earlier findings, suggesting that these novel compounds with azocine and imidazole rings should serve as scaffolding for the development of new benzazocine kinase inhibitors.

Supporting Information

The experimental FTIR spectra [Fig F1 and F2], tables for the optimized parameters [T1(a) & T1(b)], tables for the vibrational assignments [T2(a) & T2(b)] and tables for the Fukui parameters [T3(a) & T3(b)] of the title compounds NAOP-12 and NEMKH-12 have been provided in the "supplementary information file".

Acknowledgments

The help received from Prof. Neeraj Misra in the calculations is deeply acknowledged by the authors

Author Contributions

Tanveer Hasan: Conceptualization, Formal analysis, Investigation, Methodology, Software, Validation, Writing – original draft, Writing – review & editing**. Raza Murad Ghalib:** Data curation, Formal analysis, Funding acquisition. **Sayed Hasan Mehdi:** Data curation, Methodology, Resources, writing—review and editing. **Tazeem:** Investigation, Visualization, and Writing – review & editing. **Nazia Kazmi:** Writing – original draft.

References and Notes

[1] Mertens, F.; Johansson, B.; Fioretos, T.; Mitelman, F. *Nat. Rev. Cancer* **2015**, *15*, 371. [Crossref]

[2] Claudiani, S.; Apperley, J. F. *Hematology Am. Soc. Hematol. Educ. Program.* **2018**, *30*, 161. [Crossref]

[3] Schmoellerl, J.; Barbosa, I. A. M.; Eder, T.; Brandstoetter, T.; Schmidt, L.; Maurer, B.; Troester, S.; Pham, H. T. T.; Sagarajit, M.; Ebner, J.; Manhart, G.; Aslan, E.; Terlecki-Zaniewicz, S.; Van der Veen, C.; Hoermann, G.; Duployez, N.; Petit, A.; Lapillonne, H.; Puissant, A.; Itzykson, R.; Moriggl, R.; Heuser, M.; Meisel, R.; Valent, P.; Sexl, V.; Zuber, J.; Grebien, F. *Blood.* **2020**, *136*, 387. [Crossref]

[4] Katritzky, A. R.; Rees, C. W.; Scriven, E. F. V. Comprehensive Heterocyclic Chemistry ISBN 978-0-08-096518-5, Reference Work, 1996.

[5] Giraud, F.; Bourhis, M.; Nauton, L.; Théry, V.; Herfindal, L.; Døskeland, S.O.; Anizon, F.; Moreau, P. *Bioorg. Chem.* **2014**, *57*, 108. [Crossref]

[6] Ghalib, R. M.; Hashim, R.; Sulaiman, O.; Jawad, A.; Mehdi, S. H.; Bogdanovic, G. A.; Trifunovic, S. R.; Kawamura, F.; Ahamed, B. M. K.; Majid, A. M. S. A. *Cur. Org. Synt.* **2017**, *14*, 127. [Crossref]

[7] Frisch, M. J.; Trucks, G. W.; Schlegel, H. B.; Scuseria, G. E.; Robb, M. A.; Cheeseman, J. R.; Montgomery, Jr., J. A.; Vreven, T.; Kudin, K. N.; Burant, J. C.; Millam, J. M.; Iyengar, S. S.; Tomasi, J.; Barone, V.; Mennucci, B.; Cossi, M.; Scalmani, G.; Rega, N.; Petersson, G. A.; Nakatsuji, H.; Hada, M.; Ehara, M.; Toyota, K.; Fukuda, R.; Hasegawa, J.; Ishida, M.; Nakajima, T.; Honda, Y.; Kitao, O.; Nakai, H.; Klene, M.; Li, X.; Knox, J. E.; P. Hratchian, H.; Cross, J. B.; Adamo, C.; Jaramillo, J.; Gomperts, R.; Stratmann, R. E.; Yazyev, O.; Austin, A. J.; Cammi, R.; Pomelli, C.; Ochterski, J. W.; Ayala, P. Y.; Morokuma, K.; Voth, G. A.; Salvador, P.; Dannenberg, J. J.; Zakrzewski, V. G.; Dapprich, S.; Daniels, A. D.; Strain, M. C.; Farkas, O.; Malick, D. K.; Rabuck, A. D.; Raghavachari, K.; Foresman, J. B.; Ortiz, J. V.; Cui, Q.; Baboul, A. G.; Clifford, S.; Cioslowski, J.; Stefanov, B. B.; Liu, G.; Liashenko, A.; Piskorz, P.; Komaromi, I.; Martin, R. L.; Fox, D. J.; Keith, T.; Alâ€Laham, M. A.; Peng, C. Y.; Nanayakkara, A.; Challacombe, M.; Gill, P. M. W.; Johnson, B.; Chen, W.; Wong, M. W.; Gonzalez, C.; Pople, J. A. et al., Gaussian 09, revision A. 02, Gaussian, Inc., Wallingford CT, **2009**.

[8] Becke, A.D. *J. Chem. Phys.* **1993**, *98*, 5648. [Crossref]

[9] Hohenberg, P.; Kohn, W. *Phys. Rev. B*. 1**964**, *136*, 864. [Crossref]

[10] Lee, C.; Yang, W.; Parr, R. G. *Phys. Rev. B*. **1988**, *37*, 785. [Crossref]

[11] Frisch, A. et al. Gaussian Inc. GaussView, Version 6;

2009.

[12] Daina, A.; Michielin, O.; Zoete, V.; SWISSADME online software. 2017.

[13] Abraham, M. et al. GROMACS 2024.4 Source code. Available at **https://doi.org/10.5281/zenodo.14016590**

[14] Valdés-Tresanco, M. S.; Valdés-Tresanco, M. E.; Valiente, P. A.; Moreno, E. *J. Chem. Theory Comput*. **2021**, *17,* 6281. **[Crossref]**

[15] Trott, O.; Olson, A. J. *J. Comp. Chem.* **2010**, *31,* 455. **[Crossref]**

[16] Jamroz, M. H.; Vibrational Energy Distribution Analysis, VEDA 4 Program, Warsaw, Poland, 2004.

[17] Pople, J. A.; Schlegel, H. B.; Krishnan, R.; Defrees, D. J.; Binkley, J. S.; Frisch, M. J. et al. *Int. J. Quant. Chem.* **1981**, *20*, 269. **[Crossref]**

[18] Karabacak, M.; Kurt, M.; Cinar, M.; Coruh, A. *Mol. Phys.* **2009**, *107*, 253. **[Crossref]**

[19]. Colthup, N. B.; Daly, L. H.; Wiberley, S. E. In Introduction to Infrared and Raman Spectroscopy (New York: Academic Press), 1990.

[20] Krishnakumar, V.; Xavier, R. J. *Spectrochim. Acta A Mol. Biomol. Spectrosc.* **2005**, *61*, 253. **[Crossref]**

[21] Chou, K. C. *Biophys. Chem.* **1984**, *20*, 61. **[Crossref]**

[22] Frohlich, H. In Biological Coherence and Response to External Stimuli (Berlin: Springer), 1988.

[23] Xu, Y.; Chu, Q.; Chen, D.; Fuentes, A. *Front. Mech. Eng.* **2021**, *7*, 744001. **[Crossref]**

[24] Fukui, K. *Science* **1982**, *218*, 747. **[Crossref]**

[25] Fleming, I. In Frontier Orbitals and Organic Chemical Reactions: John Wiley and Sons, New York, 1976.

[26] Sajan, D.; Joseph, L.; Vijayan, N.; Karabacak, M. *Spectrochim. Acta A, Mol. Biomol. Spectrosc*. **2011**, *81,* 85. **[Crossref]**

[27] Priya, Y. S.; Rao, K. R.; Chalapathi, P. V.; Veeraiah, A.; Srikanth, K. E.; Mary, Y. S.; Thomas, R. *J. Mol. Struct.* **2020**, *1203*, 127461. **[Crossref]**

[28] Rizwana, B. F.; Prasana, J. C.; Muthu, S.; Abrahama, C. S. *Comput. Biol. Chem.* **2019**, *78*, 9. **[Crossref]**

[29] Rodrigues, R. F. N.; Almeida, L. R.; Santos, F. G. D.; Carvalho Jr., P. S.; Souza, W. C.; Moreira, K. S.; Aquino, G. L. B.; Valverde, C.; Napolitano, V.; Baseia, B. *PLoS One* **2017**, *12*, e0175859. **[Crossref]**

[30] Sharnabasappa, K.; Megha, J.; Prakash, B.; Prafulla, C.; Gajanan, R. *J. Mol. Struct.* **2018**, *1173*, 142. **[Crossref]**

[31] Thomas, R.; Mary, Y. S.; Resmi, K. S.; Narayana, B.; Sarojini, S. B. K.; Armakovic, S.; Armakovic, S. J.; Vijayakumar, G.; Alsenoy, C. V.; Mohan, B. J. *J. Mol. Struct.* **2019**, *1181*, 599. **[Crossref]**

[32] Chattaraj, P. K.; Sarkar, U.; Roy, D. R. *Chem. Rev.* **2006**, *106*, 2065. **[Crossref]**

[33] Ertl, P.; Rohde, B.; Selzer, P. *J. Med. Chem.* **2000**, *43*, 3714. **[Crossref]**

[34] Murugavel, S.; Ravikumar, C.; Jaabil, G.; Alagusundaram, P. *J. Mol. Str.* **2019**, *1176*, 729. **[Crossref]**

[35] Veber, D. F.; Johnson, S. R.; Cheng, H. Y.; Smith, B. R.; Ward, K. W.; Kopple, K. D. *J. Med. Chem.* **2002**, *45*, 2615. **[Crossref]**

[36] Zhao, Y. H.; Le, J.; Abraham, M. H.; Hersey, A.; Eddershaw, P. J.; Luscombe, C. N.; Boutina, D.; Beck, G.; Sherborne, B.; Cooper I.; Platts, J. A. *J. Pharm. Sci.* **2001**, *90*, 749. **[Crossref]**

[37] Yamashita, S.; Furubayashi, T.; Kataoka, M.; Sakane, T.; Sezaki H.; Tokuda, H. *Eur. J. Pharm. Sc.* **2000**, *10*, 195. **[Crossref]**

[38] Rodić, M. V.; Leovac, V. M.; Jovanović, L. S.; Spasojević, V.; Joksović, M. D.; Stanojković, T.; Matić, I. Z.; Vojinović-Ješić L.S.; Marković, V. *Eur. J. Med. Chem.* **2016**, *115*, 75. **[Crossref]**

[39] Lipinski, C. A.; Lombardo, F.; Dominy, B. W.; Feeney, P. J. *Adv. Drug Deliv. Rev.* **1997**, *23,* 3. **[Crossref]**

[40] Lipinski, C. A. *Drug Discov. Today Technol*. **2004**, *1*, 337. **[Crossref]**

[41] Gadaleta, D.; Vukovic, K.; Toma, C.; Lavado, G. J.; Karmaus, A. L.; Mansouri. K.; Kleinstreuer, N. C.; Benfenati, E.; Roncaglioni, A. *J. Cheminf.* **2019**, *11*, 58. **[Crossref]**

[42] Ajay, Bemis, G. W.; Murcko, M. A.; *J. Med. Chem.* **1999**, *42*, 4942. **[Crossref]**

[43] Kumar, C. P.; Raghu, M. S.; Prathibha, B. S.; Prashanth, M. K.; Kanthimathi, G.; Kumar, K. Y.; Parashuram, L.; Alharthi, F. A. *Bioorg. Med. Chem. Letters* **2021**, *44*, 128118. **[Crossref]**

[44] Spackman, P. R.; Turner, M. J.; McKinnon, J. J.; Wolff, S. K.; Grimwood, D. J.; Jayatilaka, D.; Spackman, M. A. *J. Appl. Crystallography.* **2021**, *54*, 1006. **[Crossref]**

[45] Fusion protein of heme oxygenase-1 and NADPH cytochrome P450 reductase (17aa). Available at: **http://www.rcsb.org/pdb/explore.do?structureId=6J7A&6J7I**

[46] Morris, G. M.; Huey, R.; Lindstrom, W.; Sanner, M. F.; Belew, R. K.; Goodsell, D. S.; Olson, A. J. *J. Comput. Chem.* **2009**, *16*, 2785. **[Crossref]**

[47] Schrödinger, L.; DeLano, W. 2020. PyMOL. Retrieved from **http://www.pymol.org/pymol**

[48] Biovia, D.; Berman, H.; Westbrook, J.; Feng, Z.; Gilliland, G.; Bhat, T.; Weissig, H.; Shindyalov, I.; Bourne, P.; Darden, T. *J. Chem. Phys,* **2016,** *10*, 0021.

[49] Jevtovic, V.; Alshamari, A. K.; Milenkovic, D.; Dimitrić Marković, J.; Marković, Z.; Dimić, D. *Int. J. Mol. Sci.* **2023**, *24*, 11910. **[Crossref]**

How to cite this article

Hasan, T.; Ghalib, R. M.; Mehdi, S. H.; Tazeem.; Kazmi, N. *Orbital: Electronic J. Chem*. **2025**, *17*, 35. DOI: **http://dx.doi.org/10.17807/orbital.v17i1.20314**